Acta Crystallographica Section B
Structural Science
ISSN 0108-7681

Structure refinement of a twinned pseudo-symmetric crystal of $[Mn(C_{10}H_{24}N_4)(NCO)_2]^+\cdot ClO_4^-$

Alan David Rae,[a]* Susanne Mossin[b] and Henning Osholm Sørensen[c]‡

[a]Research School of Chemistry, The Australian National University, Canberra ACT 0200, Australia, [b]Department of Chemistry, University of Copenhagen, Universitetsparken 5, 2100 Copenhagen, Denmark, and [c]Centre for Crystallographic Studies, Department of Chemistry, University of Copenhagen, Universitetsparken 5, 2100 Copenhagen, Denmark

‡ Present address: Center for Fundamental Research: Metal Structures in Four Dimensions, Risø National Laboratory, Frederiksborg 399, 4000 Roskilde, Denmark.

Correspondence e-mail: rae@rsc.anu.edu.au

Received 17 February 2005
Accepted 12 May 2005

The crystal studied is a 0.545 (1):0.455 twin, space group $C\bar{1}$, $Z = 16$, and is a commensurate occupational and displacive modulation of a $Z = 4$ idealized parent structure with the space group $A2/a$ and $\mathbf{a}_p = \mathbf{a}/2$, $\mathbf{b}_p = \mathbf{b}/2$, $\mathbf{c}_p = \mathbf{c}$. A hierarchical approach to solution and refinement led sequentially to structures in the space groups $A2/a$, $P2_1/n$, $P\bar{1}$ and finally $C\bar{1}$. The major and minor components of the reflection intensities could be identified using irreducible representations of $A2/a$ and $P2_1/n$, which in turn suggested suitable constraints and restraints for optimizing the refinement pathway. Comparative refinement was used to show the correctness of the final structure solution and how appropriately chosen constrained refinement allowed an escape from a false minima.

1. Introduction

The X-ray reflection data for crystals of $[Mn(cyclam)(NCO)_2]^+\cdot ClO_4^-$ (cyclam is the tetradentate ligand 1,4,8,11-tetraazacyclotetradecane) were consistent with the space group $C2/m$, and $Z = 16$ for the monoclinic unit cell with $a = 30.5936$ (10), $b = 18.8967$ (3), $c = 12.8288$ (5) Å, $\beta = 111.561$ (2)°. However, subset **G** of much stronger reflections was consistent with an A-centred cell with axes $\mathbf{a}_p = \mathbf{a}/2$, $\mathbf{b}_p = \mathbf{b}/2$, $\mathbf{c}_p = \mathbf{c}$ and $Z = 4$. The **G** reflections correspond to the $h = 2N$, $k = 4N$, $l = 2N$ and the $h = 2N$, $k = 4N + 2$, $l = 2N + 1$ reflections. Using only these reflections, and re-indexing them as $h_p = h/2$, $k_p = k/2$, $l_p = l$, a parent structure in space group $A2/a$ can be readily determined. In this structure the cation is apparently ordered and lies on a centre of inversion, whereas the anion is disordered about a twofold axis. The true structure is a commensurate modulation of this parent structure. Doubling the $\mathbf{a}_p$ and $\mathbf{b}_p$ axes of this parent structure necessarily destroys the glide planes and screw axes of the parent structure, thus reducing the symmetry to $C\bar{1}$. However, these pseudo-symmetry elements offer an explanation for the twinning that relates reflections hkl and $\bar{h}k\bar{l}$. This paper details how a hierarchical approach to refinement and the identification of symmetrized components of the structure creates a logical path for sensible refinement.

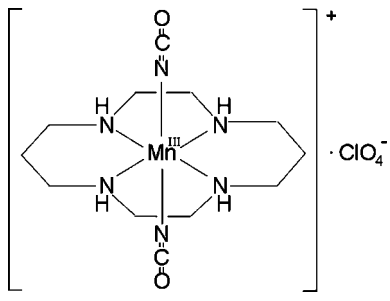

Table 1
Experimental details.

Crystal data	
Chemical formula	$C_{12}H_{24}MnN_6O_2\cdot ClO_4$
M_r	438.76
Cell setting, space group	Triclinic, $C\bar{1}$
a, b, c (Å)	30.5936 (10), 18.8967 (3), 12.8288 (5)
α, β, γ (°)	90.180 (2), 111.561 (2), 90.083 (2)
V (Å^3)	6897.9 (4)
Z	16
D_x (Mg m^{-3})	1.690
Radiation type	Mo $K\alpha$
No. of reflections for cell parameters	976
θ range (°)	4.0–33.3
μ (mm^{-1})	0.97
Temperature (K)	122 (1)
Crystal form, colour	Block, yellow–green
Crystal size (mm)	0.39 × 0.27 × 0.18
Data collection	
Diffractometer	Nonius KappaCCD
Data collection method	ω scans with κ offsets
Absorption correction	None
No. of measured, independent and observed reflections	152 267, 27 998, 17 584
Criterion for observed reflections	$I > 3\sigma(I)$
R_{int}	0.065
θ_{max} (°)	34.6
Range of h, k, l	$-48 \Rightarrow h \Rightarrow 48$ $-30 \Rightarrow k \Rightarrow 30$ $-20 \Rightarrow l \Rightarrow 20$
Refinement	
Refinement on	F
$R[F^2 > 2\sigma(F^2)]$, $wR(F^2)$, S	0.041, 0.061, 1.31
No. of reflections	27 998
No. of parameters	497
H-atom treatment	Constrained to parent site
Weighting scheme	$w = 1/[\sigma^2(F_o) + (0.02F_o)^2]$
$(\Delta/\sigma)_{max}$	0.1
$\Delta\rho_{max}$, $\Delta\rho_{min}$ (e Å^{-3})	1.00, −1.01

Computer programs used: *COLLECT* (Nonius, 1999), *DIRAX* (Duisenberg, 1992), *EvalCCD* (Duisenberg *et al.*, 2003), *DREAD* (Blessing, 1987), *SHELXS*97 (Sheldrick, 1997), *RAELS*2000 (Rae, 2000), *SIR*97 (Altomare *et al.*, 1999).

1.1. Chemical background

Manganese(III) ions seem to be a vital ingredient in several single-molecule magnets (Barra *et al.*, 1997; Long, 2003) in terms of supplying these with a high-spin ground state and the magnetic anisotropy which is a prerequisite for these magnets to exhibit their special properties. In an attempt to correlate the magnetic anisotropy of axial Mn^{III} ions to their structure and composition we have synthesized a number of new cations having the general formula *trans*-[Mn(cyclam)X_2]$^{n+}$ (Mossin *et al.*, 2002, 2005), thus providing a comprehensive series (Daugherty *et al.*, 1991; Meyer *et al.*, 1998). X is a neutral or anionic ligand. The title compound is a member of this series.

2. Experimental

2.1. Synthesis and characterization

2.1.1. *trans*-cyclambis(isocyanato)manganese(III) perchlorate, *trans*-[Mn(cyclam)(NCO)$_2$]ClO$_4$. *trans*-[Mn(cyclam)$(H_2O)_2$]$(CF_3SO_3)_3\cdot H_2O$ (0.38 g, 0.50 mmol; Mossin *et al.*, 2005) was dissolved in acetonitrile (5 ml) in a reaction tube. $NaClO_4\cdot H_2O$ (0.21 g, 1.5 mmol) and NaNCO (0.08 g, 1.2 mmol) was dissolved in a minimum amount of water and the aqueous solution was placed carefully with a Pasteur pipette in the bottom of the reaction tube containing the acetonitrile solution. Yellow–green crystals suitable for X-ray analysis appeared in the interface between the two phases. Yellow–green microcrystals were obtained by stirring the solution and filtering within minutes. The product was washed with acetonitrile and air dried. Yield: 0.18 g, 82%. Analysis: H 5.4, C 33.0, N 19.0; $H_{24}C_{12}N_6O_6ClMn$ requires: H 5.5, C 32.9, N 19.2.

The product is stable in the solid state, but decomposes slowly in aqueous solution with the evolution of gas.

Magnetic susceptibility measured at 1.3 T in the temperature interval 50–300 K on the cation [Mn(cyclam)$(NCO)_2$]$^+$ performed on [Mn(cyclam)$(NCO)_2$]CF_3SO_3 (not shown) shows a constant effective magnetic moment: μ_{eff} = 4.90 corresponding to four unpaired electrons (S = 2 ground state).

2.2. Data collection and determination of the parent structure

X-ray diffraction data were collected using a Nonius KappaCCD diffractometer employing graphite-monochromated Mo $K\alpha$ radiation on a crystal cooled to 122 (1) K. The unit cells were determined and refined by *DIRAX* (Duisenberg, 1992). Data integration and corrections for background, Lorentz and polarization effects were performed with *EvalCCD* (Duisenberg *et al.*, 2003). Data collection details are shown in Table 1.

The reflection data (152 267 reflections) were initially merged assuming $C\bar{1}$ symmetry to form a data set of 27 998 reflections, R_{merge} = 0.0652, then remerged assuming $C2/m$ diffraction symmetry to form a second data set of 15 154 reflections. For the final merge, R_{merge} was 0.0193 for the 6250 k even reflections, 0.1307 for the 6594 k odd reflections and 0.0278 for all 12 844 reflections, for which both twin components were collected. There were 699 $k \neq 0$ reflections with $I > 3\sigma(I)$, but only one of the two twin-related reflections were collected. These reflections were placed in a separate set from the other reflections. It was estimated from the merging process that an additional 6.8% error in I should be included for the k odd reflections. Initial structure solution and refinement used the second data set, thus imposing an exact 1:1 twin on the triclinic $C\bar{1}$ structure. The final refinement used the larger data set and showed that the crystal was a 0.545 (1):0.455 twin. The parent structure was solved in the space group $A2/a$ by direct methods using the program *SIR*97 (Altomare *et al.*, 1999) and refined with *SHELXL*97 (Sheldrick, 1997). Spot splitting was not observed, although an unconstrained unit-cell determination gave α = 90.180 (2) and γ = 90.083 (2)°. Reflections were processed assuming $\alpha = \gamma$ = 90.0 ° for the initial refinements, but the measured cell was used for the evaluation of geometry for the final refinement. No noticeable difference in refinement statistics resulted from changing cells and the bond-length ranges remained essentially the same.

2.3. Hierarchical structure solution and refinement

Reflections **G** are associated with a parent structure and correspond to the $h = 2N$, $k = 4N$, $l = 2N$ and the $h = 2N$, $k = 4N + 2$, $l = 2N + 1$ reflections. There are satellite reflections $\mathbf{G} \pm \mathbf{q}$ described by $h = 2N + 1$, $k = 4N \pm 1$, $l = 2N$ or $2N + 1$, implying $\mathbf{q} = \mathbf{a}^* + \mathbf{b}^* = (\mathbf{a}_p^* + \mathbf{b}_p^*)/2$, and satellite reflections $\mathbf{G} + \mathbf{q}'$ defined by $h = 2N$, $k/2 + l = 2N + 1$, implying $\mathbf{q}' = \mathbf{b}_p^*$. The satellites $\mathbf{G} + \mathbf{q}'$ can be regarded as second-order satellites since $\mathbf{G} + 2\mathbf{q}$ define the same reflections as $\mathbf{G} + \mathbf{q}'$. Omitting the h odd, k odd reflections, there are pseudo-absence conditions consistent with the cell $\mathbf{a}_p$, $\mathbf{b}_p$, $\mathbf{c}_p$ and the space group $P2_1/n$, a subgroup of $A2/a$, *i.e.* $0k0$, $k = 4n$ only and $h0l$, $h/2 + l = 2N$ only. The origin chosen for $A2/a$ located an inversion at the origin for the subgroup $P2_1/n$.

The satellite reflections $\mathbf{G} \pm \mathbf{q}$ cause a doubling of the **a** and **b** axes compared with the parent structure. This implies that all the glide operations and all the 2_1 screw operations of the $A2/a$ parent structure cannot remain true symmetry operations. An ordering of the cations is possible in a number of subgroups of $A2/a$. If we describe the parent structure in its non-standard $A2/a$ setting (a glide at $y = 0$ and inversion at the origin) and obtain the fractional coordinates for the C-centred cell as $x = x_p/2$, $y = y_p/2$, $z = z_p$, then these subgroups are $A\bar{1}$; Aa; $P2_1/n$ ($\bar{1}$ at 0,0,0 or $0,\frac{1}{4},0$); $P2_1/a$ ($\bar{1}$ at $0,\frac{1}{8},\frac{1}{4}$ or $0,\frac{3}{8},\frac{1}{4}$); $C\bar{1}$ ($\bar{1}$ at 0,0,0 or $0,\frac{1}{4},0$) and $C\bar{1}$ ($\bar{1}$ at $0,\frac{1}{8},\frac{1}{4}$ or $0,\frac{3}{8},\frac{1}{4}$), where all the fractional coordinates are described relative to the final C-centred cell and not the parent cell. *This description of fractional coordinates will be continued throughout this paper*. It should be noted that there are other subgroups of $A2/a$ which are consistent with the observed reflections, namely $A2$; $P2/a$ ($\bar{1}$ at 0,0,0 or $0,\frac{1}{4},0$); $P2/n$ ($\bar{1}$ at $0,\frac{1}{8},\frac{1}{4}$ or $0,\frac{3}{8},\frac{1}{4}$) and $C2$ (2 at $\frac{1}{8},y,0$ or $\frac{3}{8},y,0$). We have used non-standard settings for some space groups so that all the space group choices are a simple selection from the symmetry elements of the parent structure with no cell or fractional coordinate transformations required. This results in the non-standard setting of $C\bar{1}$ rather than $P\bar{1}$ for the final structure.

Irreducible representation theory (Bradley & Cracknell, 1972) can be used to assess the possible symmetries of the Fourier transform of all reflections $\mathbf{G} + n\mathbf{q}$ for a particular value of n. **G** is a Bragg reflection of the parent structure and **q** is the modulation wavevector described above. An irreducible representation associated with the vector $n\mathbf{q}$ *only* involves the parent structure symmetry element $(\mathbf{R}_m,\mathbf{t}_m)$, where $(\mathbf{R}_m,\mathbf{t}_m)\mathbf{r} = \mathbf{R}_m\mathbf{r} + \mathbf{t}_m$ if $n(\mathbf{R}_\mathrm{m}\mathbf{q} - \mathbf{q})$ is a Bragg reflection of the parent structure. Thus, all symmetry elements of the parent are involved when $n = 0$ or 2, but when $n = 1$, the only symmetry elements involved are those for which $\mathbf{R}_m = \mathbf{1}$, the identity.

However, it is possible to have either $C2$ (2 at $0,y,\frac{1}{8}$ or $0,y,\frac{3}{8}$) or $C\bar{1}$ ($\bar{1}$ at 0,0,0 or $0,\frac{1}{4},0$ or $0,\frac{1}{8},\frac{1}{4}$ or $0,\frac{3}{8},\frac{1}{4}$) as the maximum symmetry if we look at the Fourier transform of all reflections $\mathbf{G} + \mathbf{R}_m\mathbf{q}$ for all $\mathbf{R}_m$ of the parent structure. If we decide that the parent structure is $P2_1/n$, a subgroup of $A2/a$ with the same cell $\mathbf{a}_p$, $\mathbf{b}_p$, $\mathbf{c}_p$, then all $(\mathbf{R}_m\mathbf{q} - \mathbf{q})$ are now Bragg reflections of the $P2_1/n$ structure and we now only have first-order satellites. In this instance, $C\bar{1}$ ($\bar{1}$ at 0,0,0 or $0,\frac{1}{4},0$) are the maximum symmetries possible for the resulting structure.

Occupancy and displacive modes have different characteristics in a diffraction pattern. Using a Taylor expansion starting from structure factors for the idealized 1:1 disordered $A2/a$ parent structure we can say the correct structure has $F(\mathbf{H}) = [\mathrm{F}(\mathbf{H})]_o + \Sigma_i[\partial F(\mathbf{H})/\partial p_i]_o[p_i - (p_i)_o]$ + higher-order terms. The subscript o implies evaluation using the idealized parent structure. On average, at low $\sin\theta/\lambda$, $[\partial F(\mathbf{H})/\partial p_i]_o$ is large when p_i is an occupancy parameter, but small when p_i is a displacive parameter and as $\sin\theta/\lambda$ increases, $[\partial F(\mathbf{H})/\partial p_i]_o$ decreases when p_i is an occupancy parameter, but increases when p_i is a displacive parameter. Inspection of synthetic plots of undistorted reciprocal space obtained from the raw diffraction images (Nonius, 1999) showed that the occupancy was most probably associated with the second-order satellites and the displacive mode with the first-order satellite reflections.

The pseudo-absence conditions mentioned earlier suggested that it was possible to refine an apparently ordered $Z = 4$ structure in the space group $P2_1/n$ using only the h even, k even subset of observed reflections. This was found to be the case. In this model all the anions are equivalent and all the cations lie on inversion centres. However, two n-glide-related cations are not equivalent to the other two n-glide related cations. Should the symmetry be lowered to $C\bar{1}$ we then have $Z = 16$ and the first two cation sites become four non-equivalent inversion centres at $\frac{1}{2},0,0$; $\frac{1}{2},\frac{1}{2},0$; $\frac{3}{4},\frac{1}{4},\frac{1}{2}$; $\frac{3}{4},\frac{3}{4},\frac{1}{2}$ plus C-centring, while the second two cation sites become two non-equivalent general positions at $\frac{1}{2},\frac{1}{4},\frac{1}{2}$; $\frac{3}{4},\frac{1}{2},0$ plus C-centring and inversion through the origin. The four equivalent positions for the anions in $P2_1/n$ now become four non-equivalent general positions plus C-centring and inversion through the origin.

However, there is an intermediate stage that needs to be considered. The $P2_1/n$ symmetry can be lowered to $P\bar{1}$, $Z = 4$, in the cell $\mathbf{a}_p$, $\mathbf{b}_p$, $\mathbf{c}_p$ before further lowering the symmetry to $C\bar{1}$ in the larger cell **a**, **b**, **c**. In the $P\bar{1}$ space group, four non-equivalent cations each lie on an inversion centre and one pair of inversion-related anions is not equivalent to the other pair. This creates two symmetrized components in addition to the $A2/a$ and $P2_1/n$ components of the $P2_1/n$ structure. The labelling of symmetrized components is described in the *Appendix*. These components have $A\bar{1}$ and $P2/a$ symmetry and are only observed on their own in $h0l$ reflections that violate the n-glide absence condition, $h/2 + l = 2N + 1$ and, in the case of $P2/a$, the screw-axis condition $0k0$, $k = 4N + 2$. For the $A\bar{1}$ component, only 13 of the $h0l$, $h = 4N + 2$, l even reflections have $I > 3\sigma(I)$ and for the $P2/a$ component only 15 of the $h0l$, $h = 4N$, l odd reflections have $I > 3\sigma(I)$ and only the 0, 18, 0 of the $0k0$, $k = 4N + 2$ reflections has $I > 3\sigma(I)$. This compares with the 158 $h0l$, $h = 4N + 2$, l odd reflections with $I > 3\sigma(I)$ that see the $P2_1/n$ component in isolation.

Since the crystal being studied was initially assumed to be a 1:1 twin, the reliability of the $A\bar{1}$ and $P2/a$ components could only be assured if a sensible hierarchical approach to constrained refinement was adapted. First a $P2_1/n$ structure was obtained, then a $P\bar{1}$ structure and finally a $C\bar{1}$ structure.

Table 2
Refinement statistics.

Reflections were divided into classes.

Class 1	h even, $k + 2l = 4N$. $A2/a$ and $A\bar{1}$ modes.
Class 2	h even, $k + 2l = 4N + 2$. $P2_1/n$ and $P2/a$ modes.
Class 3	h odd, k odd. $C\bar{1}$ and $C\bar{1}$ modes.
Class 4	$k = 0$, l even, $h = 4N + 2$. $A\bar{1}$ mode alone.
Class 5	$k = 0$, l odd, $h = 4N + 2$. $P2_1/n$ mode alone.
Class 6	$k = 0$, l odd, $h = 4N$. $P2/a$ mode alone.
Class 7	$h = l = 0$, $k = 4N + 2$. $P2/a$ mode alone.
Class 8	$k \neq 0$ and only 1 of 2 twin-related reflections collected.
Class 9	reflections with $I < 3\sigma(I)$.
Class 1–8	reflections with $I > 3\sigma(I)$.

Reflections in classes 8 and 9 were not used in the refinement.
Reflections in classes 4–9 were excluded from classes 1–3.

Final refinement in the $C\bar{1}$ data set.

The constrained and restrained refinement in $C\bar{1}$ using 498 variables and 56 restraints. $\langle|F^2|\rangle$ values scaled relative to 1000 for Class 1. Maximum shift/sigma = 0.1. Final difference map electron density −1.00 to 1.01 e Å^{-3}. The structure contains 106 non-H-atom sites and 96 H-atom sites in the asymmetric unit.

Class	Number	$R(F)$	$R(F^2)$	wR	GoF	$\langle\|F^2\|\rangle$
1	5773	0.029	0.048	0.043	1.49	1000
2	4512	0.044	0.064	0.052	1.40	197
3	7112	0.072	0.117	0.076	1.43	64
4	13	0.204	0.323	0.289	2.70	17
5	158	0.035	0.054	0.052	1.64	361
6	15	0.227	0.377	0.356	3.79	17
7	1	0.130	0.277	0.130	1.07	14
1–7	17 584	0.041	0.055	0.054	1.43	408
9	10 414	0.533	0.765	0.364	1.04	9
All	27 998	0.086	0.064	0.061	1.31	257

Refinement statistics for the $C2/m$ data set.

Constrained and restrained refinement in $C\bar{1}$ using 497 variables.

Class	Number	$R(F)$	$R(F^2)$	wR	GoF
1	2840	0.025	0.044	0.039	1.46
2	2197	0.036	0.054	0.043	1.29
3	3616	0.056	0.094	0.062	1.21
4	13	0.158	0.234	0.261	2.48
5	158	0.035	0.054	0.051	1.61
6	15	0.209	0.334	0.332	3.59
7	1	0.054	0.110	0.054	0.45
8	699	0.065	0.093	0.069	1.58
1–8	9539	0.036	0.050	0.047	1.32
9	5615	0.399	0.608	0.343	1.02
All	15 154	0.072	0.058	0.054	1.24

Constrained refinement in $C\bar{1}$ using 365 variables.

Class	Number	$R(F)$	$R(F^2)$	wR	GoF
1	2840	0.025	0.045	0.040	1.51
2	2197	0.038	0.057	0.045	1.35
3	3616	0.074	0.126	0.088	1.71
4	13	0.480	0.697	0.425	4.00
5	158	0.036	0.055	0.053	1.66
6	15	0.415	0.596	0.624	6.70
7	1	0.365	0.863	0.365	3.04
8	699	0.066	0.093	0.070	1.59
1–8	9539	0.040	0.053	0.056	1.56
9	5615	0.417	0.640	0.365	1.08
All	15 154	0.078	0.061	0.062	1.42

Constrained refinement in $P2_1/n$. Reflections in sets 3, 4, 6 and 7 calculate as 0.0.

Class	Number	$R(F)$	$R(F^2)$	wR	GoF
1	3117	0.101	0.145	0.178	3.791
2	2336	0.272	0.430	0.361	6.489
5	158	0.277	0.466	0.444	8.949

Constrained refinement in $P\bar{1}$. Reflections in set 3 were calculated as 0.0.

Class	Number	$R(F)$	$R(F^2)$	wR	GoF
1	3117	0.087	0.124	0.146	3.126
2	2336	0.153	0.239	0.216	3.892
4	13	0.261	0.454	0.435	3.739
5	158	0.138	0.208	0.234	4.737
6	15	0.399	0.609	0.492	4.798
7	1	0.829	0.971	0.829	6.630

An uncorrelated 2% error in $|F(\mathbf{h})|$ was included along with a counting statistics error for evaluating weights $w = 1/[\sigma(F)^2 + (0.02F)^2)]$. Refinement was on F. The use of this weight modification is the cause of the GoF values being better for the $C2/m$ merged reflections. The $P2_1/n$ and $P\bar{1}$ refinements used an uncorrelated 4% error in $|F(\mathbf{h})|$ and reflections in class 9 were included in classes 1–3.

Reflections were monitored using different classes, see Table 2, in order to meaningfully assess the progress of the refinement. All refinements were carried out using the $C\bar{1}$ space group with $Z = 16$ and constraints imposed the various space-group symmetries using the comprehensive constrained least-squares refinement program *RAELS*2000 (Rae, 2000).

The $A2/a$ structure solution was used to create an initial $Z = 16$ model in space group $C\bar{1}$ in which the cations were constrained to have $A2/a$ symmetry and the anions were ordered and had $P2_1/n$ symmetry, both modulo the cell $\mathbf{a}_p$, $\mathbf{b}_p$, $\mathbf{c}_p$. All ions were described using refineable local orthonormal coordinates relative to refineable local orthonormal axial systems (Rae, 1975*a*); those for the cations were centred on the relevant Mn atom and those for the anions on the relevant Cl atom. Exact inversion for the cations was imposed either by a crystallographic inversion centre of $C\bar{1}$ or a local inversion centre using a multi-axis description available as a standard option in *RAELS* and described previously (Haller *et al.*, 1995; Rae & Willis, 2003). Atoms equivalent under $P2_1/n$ symmetry referenced the same local coordinates as a way of imposing identical object constraints. The anisotropic atom displacement parameters for each anion were described using a refineable 15-parameter *TLX* model (Rae, 1975*b*) initially centred on the relevant Cl atom. Those for the cations were described using refineable 12-parameter *TL* models centred on the relevant Mn atom. Refineable parameters were coupled together (Rae, 1984) in order to maintain the imposed symmetry. Additional individual anisotropic atom displacement parameters were defined relative to the refinable axial systems defining each cation for all the non-hydrogen cation atoms other than the Mn atoms, and these additional parameters were constrained to be exactly equal for atoms related by the $A2/a$ parent symmetry. H atoms were imposed in chemically sensible positions after each refinement cycle and

Table 3
Ranges of pseudo-equivalent cation bond lengths (Å).

Mn*n*—N*n*1	2.032 (2)–2.050 (2)
Mn*n*—N*n*2	2.036 (2)–2.041 (2)
Mn*n*—N*n*3	2.142 (2)–2.155 (2)
N*n*1—C*n*1	1.477 (3)–1.485 (3)
N*n*1–C*n*2	1.478 (3)–1.483 (3)
N*n*2–C*n*4	1.475 (3)–1.481 (3)
N*n*2–C*n*5	1.481 (3)–1.493 (3)
C*n*1–C*n*5	1.499 (3)–1.513 (3)
C*n*2–C*n*3	1.512 (3)–1.519 (3)
C*n*3–C*n*4	1.508 (3)–1.522 (3)
N*n*3–C*n*6	1.171 (3)–1.181 (3)
C*n*6–*n*1	1.193 (3)–1.202 (3)

given anisotropic displacement parameters determined by the parameters of the atoms to which they are attached.

Ordering the anions to initiate the $P2_1/n$ refinement allows a choice between two orientations for the reference anion and this corresponds to an origin choice between sites which are $(\mathbf{b}_p + \mathbf{c}_p)/2 = (\mathbf{b} + 2\mathbf{c})/4$ apart for the same structure. The orientation was chosen so that after refinement a cation with the largest principal libration axis was at the origin. We note that molecules separated by $\mathbf{b}/2$ can rotate in opposite directions upon changing to a $C\bar{1}$ structure if they both lie on inversion centres, whereas centrosymmetric molecules related by an inversion are necessarily parallel to each other.

In the $P2_1/n$ model cations 1, 2, 4, 5 at $\frac{1}{2},0,0$; $\frac{1}{2},\frac{1}{2},0$; $\frac{3}{4},\frac{1}{4},\frac{1}{2}$ and $\frac{3}{4},\frac{3}{4},\frac{1}{2}$ are equivalent; cations 3, 6 at $\frac{1}{2},\frac{1}{4},\frac{1}{2}$ and $\frac{3}{4},\frac{1}{2},0$ are equivalent, and all the anions are equivalent. The $P\bar{1}$ refinement was initiated from the $P2_1/n$ model by rotating cations 1 and 2 an equal amount about the **b** direction and the pseudo-2_1 screw-related cations 4 and 5 by an equal but opposite amount so as to destroy the screw axis. In this $P\bar{1}$ model only those reference cations and anions related by a 1/2**b** translation are equivalent. Initially the $P2_1/n$ equivalence of the rigid-body *TL* and *TLX* parameterizations was maintained, but this was later replaced by equivalence under $P\bar{1}$ symmetry. This refinement behaved fairly well and refinement improved substantially, initially quite slowly but more rapidly after each cycle until eventual convergence. Refinement statistics are given in Table 2.

Examination of the final $P\bar{1}$ model showed that the anions and the cations 3 and 6 maintain equivalence under $P2_1/n$ symmetry to a very good approximation. Also, cations 1 and 2 and cations 4 and 5 had very similar libration parameters with one large principal value of *ca* 0.075 radians^2, corresponding to a root mean-square displacement of *ca* 15 ° in directions roughly equivalent under $P2_1/n$ symmetry. This suggests the major contribution to the $C\bar{1}$ reflections is a displacive mode in which these four cations each rotate by equal amounts about their major principal libration axis direction, with the displacements being equal but opposite for cations 1 and 2 (and for cations 3 and 4). However, the rotations for cations 1 and 3 are either equal or opposite. These options correspond to the different orientations of the same displacive mode, *i.e.* either $C\bar{1}^{\rm i}$ or $C\bar{1}^{\rm ii}$ (see the *Appendix*). However, the distinction between orientations has already been made by the $P\bar{1}$ component and so both options had to be attempted. The overall sign of this component selects between alternative origins. In an initial refinement cycle of comparative constrained refinements (see the *Appendix*) the $C\bar{1}^{\rm ii}$ option, based on the reference cation site $x,y,z = \frac{1}{2},0,0$, performed better and this model was refined. The existence of finite $P\bar{1}$ and $C\bar{1}^{\rm ii}$ components initiated refinement of the $C\bar{1}^{\rm i}$ component and the contributions from the remaining ions to the $C\bar{1}$ components. The definition of the $C\bar{1}^{\rm ii}$ component was chosen to include the major contribution from each set of pseudo-equivalent ions at x,y,z; $x,y+\frac{1}{2},z$; $-x+\frac{1}{4},y+\frac{1}{4},-z+\frac{1}{2}$ and $-x+\frac{1}{4},y+\frac{3}{4},-z+\frac{1}{2}$) by appropriately selecting the ion site for the reference equivalent position x,y,z (see the *Appendix*).

To restrict the possible noise in the less well determined $P\bar{1}$ and $C\bar{1}^{\rm i}$ components each pair of pseudo-equivalent cation positions, *viz.* ($x,y,z = \frac{1}{2},0,0$ and $-x+\frac{1}{4},y+\frac{3}{4},-z+\frac{1}{2}$),($x, y+\frac{1}{2},z$ and $-x+\frac{1}{4},y+\frac{1}{4},-z+\frac{1}{2}$), ($x,y+\frac{1}{4},z+\frac{1}{2}$ and $-x+\frac{1}{4},y,-z$), ($x,y+\frac{3}{4},z+\frac{1}{2}$ and $-x+\frac{1}{4},y+\frac{1}{2},-z$), was constrained to have their local coordinates in common. (In the atom list the last two pseudo-equivalent positions were replaced by their $C\bar{1}$ equivalents $-x$, $-y+\frac{1}{4}$, $-z+\frac{1}{2}$ and $x+\frac{1}{4}$, $-y$, z.) Initially the $P\bar{1}$ equivalence of the *TL* and *TLX* parameterizations was maintained, but this equivalence was later removed. The anions were not constrained to have local symmetry but were initially constrained to have the same local coordinates so as to maintain a pseudo-equivalence under $P2_1/n$ symmetry because of their small contribution to the k odd reflections. Pairs of pseudo-equivalent anions at $x,y,z \simeq \frac{5}{8},y,0$ and $-x+\frac{1}{4},y+\frac{3}{4},-z+\frac{1}{2}$ ($y \simeq 0.19$ or 0.69) were subsequently constrained to have their local coordinates in common. Final refinement of this model used 365 variables and refined to give $R(F) = 0.040$ for the 9539 independent merged reflections with $I > 3\sigma(I)$ obtained assuming $C2/m$ diffraction symmetry. This model was rerun excluding the 699 $k \neq 0$ reflections for which only one of two twin equivalents was collected. This had almost no effect on the refinement statistics other than increasing the $R(F)$ value for these reflections from 0.063 to 0.066 (*GoF* from 1.52 to 1.59). Further details are given in Table 2.

The only change for the final refinement cycles of the $C2/m$ merged reflections was to refine all non-H atoms independently, thus increasing the number of variables to 497. The number of restraints on the distance differences used was now 56. Bond lengths constrained to be equal in the previous model were now only restrained to approach equality. The final statistics on the h odd, k odd reflections (excluding reflections for which only one of the two twin equivalents was collected) were now $R(F) = 0.057$ compared with 0.074 and $GoF = 1.21$ compared with 1.34. The success of the final refinement was so good that replacing the rigid-body parameterization with an individual atom displacement parameterization was considered to be unnecessary.

Refinement was then transferred to the larger set of reflections merged assuming $C\bar{1}$ diffraction symmetry. A twin ratio of 0.545 (1):0.455 was obtained using 498 variables to describe 96 non-H-atom sites and 106 H-atom sites. These results were used in the lists of atom parameters, bond lengths and bond angles. Refinement statistics are in Table 2. It should be noted that the relative importance of the *h0l* reflections in

evaluating the minor modes is reduced when the twin ratio is no longer 0.5:0.5.

3. Results and discussion

The ranges of pseudo-equivalent cation bond lengths are given in Table 3. The use and labelling of symmetrized components is described in the *Appendix*. Tables 4 and 5 assume $A2/a$ is the parent symmetry, whereas Tables 6 and 7 assume $P2_1/n$ is the parent symmetry.

The structure can be described as two substructures of $C\bar{1}$ symmetry. The first substructure contains cations in a centrosymmetric layer at $x = \frac{1}{2}$ located at the inversion centres $\frac{1}{2},0,0$ and $\frac{1}{2},\frac{1}{2},0$ and the general positions $\frac{1}{2},\frac{1}{4},\frac{1}{2}$ and its inversion equivalent $\frac{1}{2},\frac{3}{4},\frac{1}{2}$. The pseudo-symmetry operation $-x + \frac{1}{4}, y + \frac{3}{4}, -z + \frac{1}{2}$ creates an almost identical layer at $x = \frac{3}{4}$. Within these layers the cations are hydrogen bonded, with N_{cyclam} as the hydrogen-bond donor and O(CN) as the acceptor, to form one-dimensional chains. The N$\cdots$O distances are in the range 2.830 (3)–2.970 (3) Å. At the interface at $x = 5/8$, anions 1 and 2 at $\sim$ 0.62,0.19,−0.02 and 0.62 0.69,−0.02 would appear to be associated with the first substructure and anions 3 and 4 at $\sim$ 0.63,0.94,−0.02 and 0.63,0.44,−0.02 with the second. Only one O atom on each anion, *viz.* O15, O25, O35 or O45, points away from the interface towards the layer of its associated substructure. The labelling of cation 3 on a general position is shown in Fig. 1. The first integer in the label distinguishes the cation. A projection down **c** of the unit cell is shown in Fig. 2.

Manganese is six-coordinate, with cyclam occupying the four equatorial positions and isocyanate in the axial positions. The cyclam ligand is found in the energetically most favourable conformation *trans*-III (Bosnich *et al.*, 1965), with bond lengths and angles similar to those of other manganese(III)-cyclam complexes (Mossin *et al.*, 2002, 2005).

The Mn—N_{cyclam} bonds in all six complexes [2.032 (2)–2.050 (2) Å] also have lengths equal to those of related manganese(III) cyclam complexes, with average Mn—N_{cyclam} bond lengths between 2.028 (2) and 2.041 (2) Å (Mossin *et al.*, 2005). The axial ligands, which are nitrogen coordinated (see discussion in the next paragraph), have Mn*n*—N*n*3 distances in the range 2.142 (2)–2.155 (2) Å. This is slightly shorter than those observed with other nitrogen donors where the average values are 2.166 (17) Å (for $[Mn(cyclam)(NCS)_2]^+$) and 2.171 (6) Å (for $[Mn(cyclam)(N_3)_2]^+$) (Daugherty *et al.*, 1991; Meyer *et al.*, 1998).

The manganese ion is a class-a acceptor ('hard' ion) and thus forms its most stable complexes with ligands containing the most electronegative donor atoms (Greenwood & Earnshaw, 1984). This effect is even more pronounced for the higher oxidation states (III, IV) of manganese found in metal-organic complexes. O is more electronegative than N and since NCO in principle can act as either an N or an O donor, we have looked more closely into the coodination mode. The bond distances in the cyanate ligands suggest that nitrogen is the donor atom. The N*n*3—C*n*6 distances are between 1.171 (3) and 1.181 (3) Å, and are thereby shorter than C*n*6—O*n*1, which are between 1.193 (3) and 1.202 (3) Å (Table 3). The relatively linear coordination mode of cyanate [average angle Mn*n*—N*n*3—C*n*6 of 160.6° with a range from 156.7 (3) to 166.5 (3)°] indicates nitrogen coordination using the Valence Shell Electron Pair Repulsion (VSEPR) model. A search for terminally bonded cyanate or isocyanate ligands to transition metals in the Cambridge Structural Database (CSD, Version 5.25, November 2003; Allen, 2002) led to 109 hits having an *R* value below 10%. Only one of these, a nickel complex, was claimed to be a cyanato complex (Vicente *et al.*, 1997), but in fact it is very unlikely that this assignment is correct. The structure is disordered, having both cyanate and

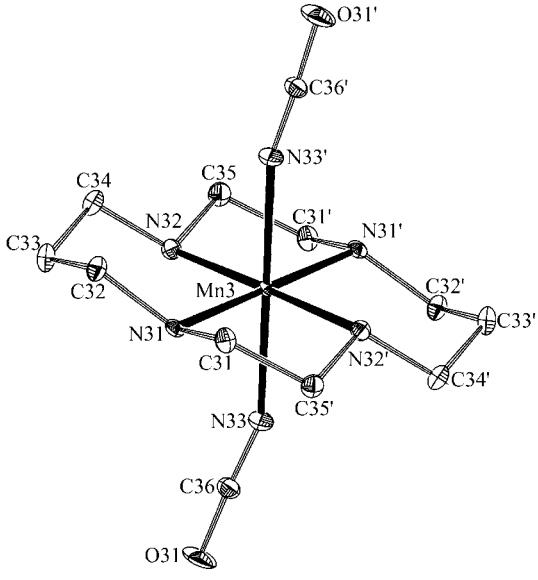

Figure 1
*ORTEP*II drawing (Johnson, 1976) showing the labelling of cation 3. Displacement ellipsoids are drawn at the 50% probability level.

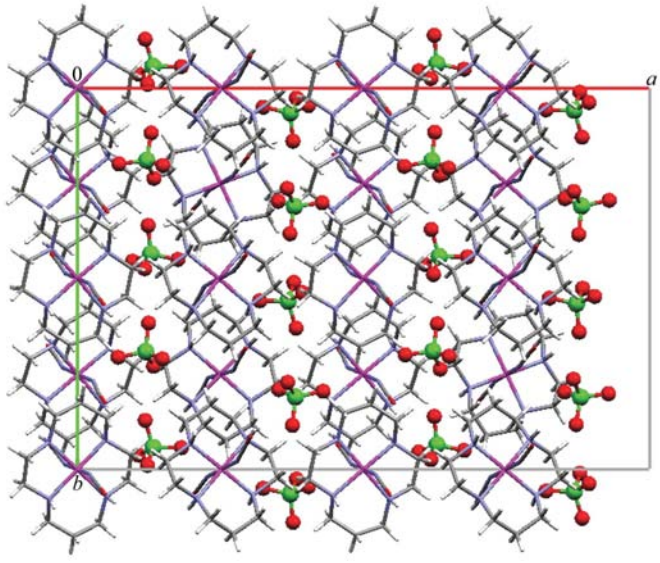

Figure 2
A projection down **c** of the unit cell.

perchlorate partially ligating in the same position, leading to some very non-physical atomic displacements in the final model. The average bond distances and angles in the cyanate ligands extracted from the CSD are in very good agreement with those found in the present structure. The average Mn—N—C angle of the extracted structures is 160.5° compared with an average value of 160.6°; for N—C—O the average angle is 177.3° compared with 177.5°. The bond distances for N—C and C—O in Mn compounds (six compounds in the literature) average 1.161 (7) and 1.201 (4) Å, respectively. This is again in close agreement with values given in Table 3. We therefore conclude that the Mn—NCO coordination mode is correct.

3.1. Comparative refinements

We described the crystal as having two nearly identical substructures of $C\bar{1}$ symmetry, the second related to the first by the pseudo-symmetry element $-x+\frac{1}{4},y+\frac{3}{4},-z+\frac{1}{2}$. If this substructure relationship were exact, then the $P\bar{1}$ and $C\bar{1}^{\rm i}$ symmetrized components would be zero. Which ions are included in the reference substructure defines the content of the $C\bar{1}^{\rm ii}$ component (see the *Appendix*). We can check the quality of a pseudo-symmetry-related substructure description by moving the second substructure by 1/2**b** relative to the first. This would be equivalent to $-x+\frac{1}{4},y+\frac{3}{4},-z+\frac{1}{2}$ acting on the whole structure if the $P\bar{1}$ and $C\bar{1}^{\rm i}$ symmetrized components were exactly zero. As can be seen from Table 6, the $C\bar{1}^{\rm ii}$ symmetrized component should then be re-labelled as $C\bar{1}^{\rm i}$. Only the statistics for h odd, k odd reflections are changed in this new model and for our substructure definition an initial $R(F)$ value of 0.293 resulted for those h odd, k odd reflections with $I > 3\sigma(I)$. The poorer statistics of these reflections compared with the initial model is the result of inadequacies in the substructure translation as a model for re-orienting the crystal. In particular, the substructure translation imposes the wrong sign for second-order terms in a Taylor expansion arising from the $P\bar{1}$ displacive mode and either of the two $C\bar{1}$ displacive modes. Since it is the $P\bar{1}$ mode and the minor $C\bar{1}$ mode that create a contribution of the same symmetry as the major $C\bar{1}$ component, the larger the $R(F)$ value of the h odd, k odd reflections in the new description, the larger the structure-factor contribution from the minor components. An alternative substructure description is to select all the ions at $z = 0$. Translating the other substructure by **b**/2 now gives an initial $R(F)$ value of 0.429 for those h odd, k odd reflections with $I > 3\sigma(I)$, *i.e.* this substructure definition is not as accurate as the previous one.

Whether these wrong structures created by a substructure translation can be refined to re-obtain the original structure transformed by the operation $-x+\frac{1}{4},y+\frac{3}{4},-z+\frac{1}{2}$ gives an indication of the robustness of our refinement procedures, *i.e.* how effectively we can reverse the sign of all the $P\bar{1}$ components of reflections $F(\mathbf{H})$, including the pseudo-systematic absences of the $P2_1/n$ parent structure that see only the $P\bar{1}$ component.

Pairs of pseudo-equivalent positions, constrained to have their local coordinates in common, should now be (x,y,z and $-x+\frac{1}{4},y+\frac{1}{4},-z+\frac{1}{2}$), ($x,y+\frac{1}{2},z$ and $-x+\frac{1}{4},y+\frac{3}{4},-z+\frac{1}{2}$), ($x,y+\frac{3}{4},z+\frac{1}{2}$ and $-x+\frac{1}{4},y,-z$), ($x,y+\frac{1}{4},z+\frac{1}{2}$ and $-x+\frac{1}{4},y+\frac{1}{2},-z$), consistent with moving one best-choice substructure by $\frac{1}{2}$**b**. If we use these local coordinate constraints, then refinement using all reflections with $I > 3\sigma(I)$ essentially recreated the original structure transformed by $-x+\frac{1}{4},y+\frac{3}{4},-z+\frac{1}{2}$, within about 4 cycles for the first model and within 9 cycles for the second. Unconstrained refinement gets lost along the way. Initial refinement of the second model was slow, with the fit of h even, k even reflections getting worse while the fit of h odd, k odd reflections got slowly better. The final statistics on the h odd, k odd reflections were not quite as good [$R(F) = 0.077$ compared with 0.074 and $Gof = 1.81$ compared with 1.71 for both pathways]. The fit of reflections that violate the $P2_1/n$ absence conditions and so only see the $P\bar{1}$ component do not fit well in any of the models and only improved when geometries previously constrained to be equal were refined independently subject to restraints that made previously equal distances only approach equality. We note that some pathway dependence is evident in the refinement. The equal object constraints that did so much for correcting the models in which substructures were wrongly related actually stops the refinements becoming equivalent. Replacing constraints by restraints at the final stage allowed all refinements to become equivalent in the 497 parameter model.

Attempts at other refinements, starting from constrained refinement models and then reverting to some form of restrained refinement, clearly showed that the best results were obtained by following a sensible constraint refinement pathway as far as possible before replacing certain constraints by sensibly chosen restraints.

APPENDIX *A*
The use of symmetrized components

The structure can be described in terms of symmetrized components. To a first approximation each displacive mode involves some combination of rigid-body rotations and translations of the cations and anions. Differences in local coordinates of the pseudo-equivalent cations or anions only become meaningfully refineable when these gross rigid-body parameters are well determined. Symmetrization can be created in two ways:

(i) by combining the structure factors of pseudo-equivalent reflections and

(ii) by combining the parameters of pseudo-equivalent atoms or ions.

Using the m = 1–32 symmetry elements ($\mathbf{R}_m,\mathbf{t}_m$) of $A2/a$ modulo the cell $\mathbf{a} = 2\mathbf{a}_p$, $\mathbf{b} = 2\mathbf{b}_p$, $\mathbf{c} = \mathbf{c}_p$, the scattering density of a mosaic block of a crystal can be symmetrized and becomes $\rho(\mathbf{r}) = \Sigma_n \rho_n(\mathbf{r})$, where the nth of 32 components is described using appropriately chosen χ_{mn} coefficients as

$$\rho_n(\mathbf{r}) = (1/32)\Sigma_m \chi_{mn} \rho(\mathbf{R}_m\mathbf{r} + \mathbf{t}_m).$$

Table 4
Values of χ_{mn} for symmetrized components using an $A2/a$ parent structure.

The superscripts a–d are used to distinguish the four $C\bar{1}$ modes. χ_{mn} has the same value for pseudo-equivalent positions related by $C\bar{1}$ symmetry.

Pseudo-equivalent Position	$A2/a$ $n = 1$	$A\bar{1}$ 2	$P2_1/n$ 3	$P2/a$ 4	$C\bar{1}^a$ 5	$C\bar{1}^b$ 6	$C\bar{1}^c$ 7	$C\bar{1}^d$ 8
x, y, z	+1	+1	+1	+1	+1	+1	+1	+1
$x, y+\frac{1}{2}, z$	+1	+1	+1	+1	−1	−1	−1	−1
$x, y+\frac{1}{4}, z+\frac{1}{2}$	+1	+1	−1	−1	$-i$	$+i$	$-i$	$+i$
$x, y+\frac{3}{4}, z+\frac{1}{2}$	+1	+1	−1	−1	$+i$	$-i$	$+i$	$-i$
$-x+\frac{1}{4}, y+\frac{1}{4}, -z+\frac{1}{2}$	+1	−1	+1	−1	+1	+1	−1	−1
$-x+\frac{1}{4}, y+\frac{3}{4}, -z+\frac{1}{2}$	+1	−1	+1	−1	−1	−1	+1	+1
$-x+\frac{1}{4}, y+\frac{1}{2}, -z$	+1	−1	−1	+1	$-i$	$+i$	$+i$	$-i$
$-x+\frac{1}{4}, y, -z$	+1	−1	−1	+1	$+i$	$-i$	$-i$	$+i$

In the atom list the last two pseudo-equivalent positions were replaced by their $C\bar{1}$ equivalents $-x, -y+\frac{1}{4}, -z+\frac{1}{2}$ and $x+\frac{1}{4}, -y, z$.

If $[1/(32)^{1/2}]\chi_{mn}$ is chosen as a unitary matrix, *i.e.* $(1/32)\Sigma_{m\,=\,1,32}\chi_{mn}\chi'^{*}_{mn} = 1$ if $n = n'$, 0 otherwise, then

$$\rho(\mathbf{R}_m\mathbf{r} + \mathbf{t}_m) = \Sigma_{n=1,32}\chi^{*}_{mn}\rho_n(\mathbf{r}).$$

Consequently, the structure factor for a mosaic block can be written as

$$F(\mathbf{H}) = \Sigma_n F_n(\mathbf{H}) \text{ and}$$
$$F(\mathbf{R}_m^{-1}\mathbf{H}) = \exp(-2\pi i\mathbf{H}\cdot\mathbf{t}_m)\Sigma_n\chi^{*}_{mn}F_n(\mathbf{H}),$$

where $F_n(\mathbf{H})$ is the Fourier transform of the component $\rho_n(\mathbf{r})$ and

$$F_n(\mathbf{H}) = (1/32)\Sigma_m\chi_{mn}\exp(2\pi i\mathbf{H}\cdot\mathbf{t}_m)F(\mathbf{R}_m^{-1}\mathbf{H}).$$

It follows that $\Sigma_n|F_n(\mathbf{H})|^2 = (1/32)\Sigma_m|F(\mathbf{R}_m^{-1}\mathbf{H})|^2$. Any twinning reduces the correlation between $F_n(\mathbf{H})$ components and 1:1 twinning (as, for example, in a powder pattern) removes the correlation altogether. Twinning that imposes exact $2/m$ diffraction symmetry for our structure implying observations of $I(\mathbf{H})$ is $\Sigma_n|F_n(\mathbf{H})|^2$ rather than $|\Sigma_n F_n(\mathbf{H})|^2$, as would apply to a perfectly ordered structure. It should be noted that the number of independent components $F(\mathbf{R}_m{}^{-1}\mathbf{H})$ for a particular $\mathbf{H}$ determines the degrees of freedom for components $F_n(\mathbf{H})$ at any $\mathbf{H}$. Coefficients χ_{mn} can be chosen so as to define the index and phase conditions that allow a component $F_n(\mathbf{H})$ to be non-zero. Stacking fault disorder could reduce the scale of some $F_n(\mathbf{H})$ components but not others. However, our final refinement showed no evidence for stacking faults.

We can label the symmetry of a component $\rho_n(\mathbf{r})$ by finding the largest subgroup of symmetry elements $(\mathbf{R}_m,\mathbf{t}_m)$ for which $\rho_n(\mathbf{R}_m\mathbf{r} + \mathbf{t}_m) = \rho_n(\mathbf{r})$. Irreducible representation theory suggests coefficients that create unique labels for singly degenerate irreducible representations. For doubly degenerate irreducible representations any linear combinations of basis functions, *e.g.* $\rho_n(\mathbf{r})$, for an irreducible representation could be used as a basis function for the same irreducible representation. This implies the coefficients χ_{mn} are not unique for such components.

Our structure has $C\bar{1}$ symmetry and consequently the only components that have $F_n(\mathbf{H}) \neq 0$ are those that have a symmetry containing $C\bar{1}$ as a subgroup. These are the $A2/a$ and $A\bar{1}$ components, which only contribute to the parent reflections, the $P2_1/n$ and $P2/a$ components which only contribute to the second-order satellite reflections, and the degenerate $C\bar{1}$ components which only contribute to the first-order satellite reflections.

These ideas were developed using the scattering density of the actual structure. The 32 equivalent positions of $A2/a$ modulo the cell $\mathbf{a} = 2\mathbf{a}_p$, $\mathbf{b} = 2\mathbf{b}_p$, $\mathbf{c} = \mathbf{c}_p$, can be written in the form $(\mathbf{R}_m,\mathbf{t}_m) = (\mathbf{1},\mathbf{t}_1)^{N1}(-\mathbf{1},\mathbf{0})^{N2}(\mathbf{1},\mathbf{t}_3)^{N3}(\mathbf{2},\mathbf{t}_4)^{N4}$, where $N3$ can be 0, 1, 2 or 3 and $N1$, $N2$, $N4$ can each be either 0 or 1, and $(\mathbf{R}_m,\mathbf{t}_m)^0$ is the identity x,y,z for any m. $(\mathbf{1},\mathbf{t}_1)$ corresponds to the translation $x+\frac{1}{2},y+\frac{1}{2},z$; $(-\mathbf{1},\mathbf{0})$ corresponds to the inverse operation $-x,-y,-z$; $(\mathbf{1},\mathbf{t}_3)$ corresponds to the translation $x,y+\frac{1}{4},z+\frac{1}{2}$; and $(\mathbf{2},\mathbf{t}_4)$ corresponds to the rotation operation $-x+\frac{1}{4},y,-z$. We can say χ_{mn} is the product of four numbers, *i.e.* $n_1(N1), n_2(N2), n_3(N3), n_4(N4)$, where $n_1(N1) = n_2(N2) = 1$ for all values of $N1$ and $N2$ so as to preserve $C\bar{1}$ symmetry with an inversion at the origin. Making $n_3(0) = n_4(0) = 1$ selects an origin and orientation. Table 4 gives possible values of χ_{mn} for symmetrized components that have been chosen so that all $|\chi_{mn}| = 1$.

The functional form ($h + k = 2N$ only) for the different symmetrized components can then be constructed from the true structure factor $F(\mathbf{H}) = A(\mathbf{H})$ for the $C\bar{1}$ structure.

$$F_1(\mathbf{H}) = 0 \text{ unless } k+2l = 4N \text{ when}$$
$$F_1(\mathbf{H}) = [A(\mathbf{H}) + \varphi A(\mathbf{2H})]/2 = \varphi F_1(\mathbf{2H})$$
$$F_2(\mathbf{H}) = 0 \text{ unless } k+2l = 4N \text{ when}$$
$$F_2(\mathbf{H}) = [A(\mathbf{H}) - \varphi A(\mathbf{2H})]/2 = -\varphi F_2(\mathbf{2H})$$
$$F_3(\mathbf{H}) = 0 \text{ unless } k+2l = 4N+2 \text{ when}$$
$$F_3(\mathbf{H}) = [A(\mathbf{H}) + \varphi A(\mathbf{2H})]/2 = \varphi F_3(\mathbf{2H})$$
$$F_4(\mathbf{H}) = 0 \text{ unless } k+2l = 4N+2 \text{ when}$$
$$F_4(\mathbf{H}) = [A(\mathbf{H}) - \varphi A(\mathbf{2H})]/2 = -\varphi F_4(\mathbf{2H})$$
$$F_5(\mathbf{H}) = 0 \text{ unless } k+2l = 4N+1 \text{ when}$$
$$F_5(\mathbf{H}) = [A(\mathbf{H}) + \varphi A(\mathbf{2H})]/2 = \varphi F_8(\mathbf{2H})$$
$$F_6(\mathbf{H}) = 0 \text{ unless } k+2l = 4N+3 \text{ when}$$
$$F_6(\mathbf{H}) = [A(\mathbf{H}) + \varphi A(\mathbf{2H})]/2 = \varphi F_7(\mathbf{2H})$$
$$F_7(\mathbf{H}) = 0 \text{ unless } k+2l = 4N+1 \text{ when}$$
$$F_7(\mathbf{H}) = [A(\mathbf{H}) - \varphi A(\mathbf{2H})]/2 = -\varphi F_6(\mathbf{2H})$$
$$F_8(\mathbf{H}) = 0 \text{ unless } k+2l = 4N+3 \text{ when}$$
$$F_8(\mathbf{H}) = [A(\mathbf{H}) - \varphi A(\mathbf{2H})]/2 = -\varphi F_5(\mathbf{2H}),$$

where $\varphi = (-1)^{(h\,+\,k\,+\,2l)/2}$.

We see that for a perfect twin $I(\mathbf{H}) = I(\mathbf{2H}) = \Sigma_n|F_n(\mathbf{H})|^2 = [|A(\mathbf{H})|^2 + |A(\mathbf{2H})|^2]/2$ for all $\mathbf{H}$. There are only two non-zero components associated with any $k + 2l$ index condition and $I(\mathbf{H}) = |F_1(\mathbf{H})|^2 + |F_2(\mathbf{H})|^2$ for the parent reflections, $|F_3(\mathbf{H})|^2 + |F_4(\mathbf{H})|^2$ for the second-order satellite reflections, $|F_5(\mathbf{H})|^2 + |F_7(\mathbf{H})|^2$ for the first-order satellite reflections with $k + 2l = 4N+1$, and $|F_5(\mathbf{2H})|^2 + |F_7(\mathbf{2H})|^2$ for the first-order satellite reflections with $k + 2l = 4N + 3$.

Table 5
Multiplication table using an $A2/a$ parent structure.

	$A2/a$	$P2_1/n$	$A\bar{1}$	$P2/a$	$C\bar{1}^a$	$C\bar{1}^b$	$C\bar{1}^c$	$C\bar{1}^d$
$A2/a$	$A2/a$	$P2_1/n$	$A\bar{1}$	$P2/a$	$C\bar{1}^a$	$C\bar{1}^b$	$C\bar{1}^c$	$C\bar{1}^d$
$P2_1/n$	$P2_1/n$	$A2/a$	$P2/a$	$A\bar{1}$	$C\bar{1}^b$	$C\bar{1}^a$	$C\bar{1}^d$	$C\bar{1}^c$
$A\bar{1}$	$A\bar{1}$	$P2/a$	$A2/a$	$P2_1/n$	$C\bar{1}^c$	$C\bar{1}^d$	$C\bar{1}^a$	$C\bar{1}^b$
$P2/a$	$P2/a$	$A\bar{1}$	$P2_1/n$	$A2/a$	$C\bar{1}^d$	$C\bar{1}^c$	$C\bar{1}^b$	$C\bar{1}^a$
$C\bar{1}^a$	$C\bar{1}^a$	$C\bar{1}^b$	$C\bar{1}^c$	$C\bar{1}^d$	$P2_1/n$	$A2/a$	$P2/a$	$A\bar{1}$
$C\bar{1}^b$	$C\bar{1}^b$	$C\bar{1}^a$	$C\bar{1}^d$	$C\bar{1}^c$	$A2/a$	$P2_1/n$	$A\bar{1}$	$P2/a$
$C\bar{1}^c$	$C\bar{1}^c$	$C\bar{1}^d$	$C\bar{1}^a$	$C\bar{1}^b$	$P2/a$	$A\bar{1}$	$P2_1/n$	$A2/a$
$C\bar{1}^d$	$C\bar{1}^d$	$C\bar{1}^c$	$C\bar{1}^b$	$C\bar{1}^a$	$A\bar{1}$	$P2/a$	$A2/a$	$P2_1/n$

Table 6
Values of χ_{mn} for symmetrized components using a $P2_1/n$ parent structure.

χ_{mn} has the same value for pseudo-equivalent positions related by $C\bar{1}$ symmetry.

Pseudo-equivalent Position	$P2_1/n$ $n = 1$	$P\bar{1}$ 2	$C\bar{1}^{i}$ 3	$C\bar{1}^{ii}$ 4
x, y, z	+1	+1	+1	+1
$x, y + \frac{1}{2}, z$	+1	+1	−1	−1
$-x + \frac{1}{4}, y + \frac{1}{4}, -z + \frac{1}{2}$	+1	−1	+1	−1
$-x + \frac{1}{4}, y + \frac{3}{4}, -z + \frac{1}{2}$	+1	−1	−1	+1

For the k even reflections each symmetrized component has a different inherent symmetry and the imposition of an overall symmetry of $A2/a$ or $P2_1/n$ makes certain $F_n(\mathbf{H})$ be zero. However, for the k odd reflections a mix of the two independent components of the same $C\bar{1}$ symmetry can be chosen so as to specify a dominant component and a minor component that helps identify constraints that would minimize the contribution of the minor component at certain stages of a refinement, see later.

A1. The use of symmetrized parameters

The Taylor expansion $F(\mathbf{H}) = [F(\mathbf{H})]_o + \Sigma_{i,m}[\partial F(\mathbf{H})/\partial p_{im}]_o [p_{im} - (p_{im})_o]$ + higher-order terms becomes a first-order approximation to the structure factors when the higher-order terms are omitted. The subscript o implies a value evaluated using an idealized parent structure and p_{im} is the actual value of the ith parameter in the mth asymmetric unit of the parent structure. The parent structure symmetry redefines the reference axes for a parameter in each asymmetric unit. We can use symmetrized parameter combinations P_{in} that span the same variable space as the atom-based parameters p_{im} with

$$[p_{im} - (p_{im})_o] = \Sigma_n \chi_{mn}[P_{in} - (P_{in})_o],$$

so that

$$F(\mathbf{H}) = [F(\mathbf{H})]_o + \Sigma_{i,n}[\partial F(\mathbf{H})/\partial P_{in}]_o[P_{in} - (P_{in})_o] + \text{higher order terms},$$

where $[\partial F(\mathbf{H})/\partial P_{in}]_o = \Sigma_m \chi_{mn}[\partial F(\mathbf{H})/\partial p_{im}]_o$, $\chi_{mn} = \partial p_{im}/\partial P_{in}$ and $[P_{in} - (P_{in})_o] = 0$ if $F_n(\mathbf{H})$ must remain zero because of the symmetry requirements of $\rho(\mathbf{r})$.

If $[1/(32)^{1/2}]\chi_{mn}$ is chosen as a unitary matrix, then

$$[P_{in} - (P_{in})_o] = (1/32)\Sigma_{m=1,32}\chi^*_{mn}[p_{im} - (p_{im})_o].$$

To a first-order approximation

$$F_n(\mathbf{H}) \simeq [F_n(\mathbf{H})]_o + \Sigma_i[\partial F(\mathbf{H})/\partial P_{in}]_o[P_{in} - (P_{in})_o]$$

and at any stage of the refinement of a perfectly twinned crystal

$$\partial[\Sigma_n|F_n(\mathbf{H})|^2]/\partial P_{in} = \Sigma_n\{F_n(\mathbf{H})^*[\partial F_n(\mathbf{H})/\partial P_{in}]_o + \text{complex conjugate}\}$$

is zero unless $F_n(\mathbf{H}) \neq 0$. The $F_n(\mathbf{H})$ components are produced from the current calculated model and so are pathway-specific. Each $n \neq 1$ component has a choice of global phase and these choices are uncorrelated for a 1:1 twinned crystal at this level of approximation. The global phase chosen for an individual component defines a choice of origin and orientation for that component. However, when taken together these choices need not simply correspond to choices of origin and orientation of the total structure. Consequently, it is easy to obtain false refinement minima. Accidental choices of wrong global phases are not necessarily self correcting, even for an untwinned crystal (Rae *et al.*, 1990), and can lead to minor $F_n(\mathbf{H})$ components of a pseudo-centrosymmetric crystal being poorly determined as well as having an incorrect global phase. A hierarchical approach to refinement restricts the contributions to the minor $F_{\rm n}(\mathbf{H})$ components in order to better determine values of $\partial[\Sigma_n|F_n(\mathbf{H})|^2]/\partial P_{in}$ so that refinement can meaningfully continue. Rigid-body models for anisotropic atom displacement parameters and the use of local orthonormal coordinates allow constraints that restrict the noise in these minor components. Constraints that certain symmetrized parameters are zero can also be imposed. Alternatively restraints that make certain symmetrized parameters approach zero can be used.

It should be noted that the second-order term of a Taylor expansion of F($\mathbf{H}$), *i.e.*

$$+\tfrac{1}{2}\Sigma_{i,i',n,n'}[\partial^2 F(\mathbf{H})/\partial P_{in}\partial P_{i'n'}]_o[P_{in} - (P_{in})_o][P_{i'n'} - (P_{i'n'})_o]$$

creates correlations between the various symmetrized components by making contributions to the components $F_n(\mathbf{H})$ according to the symmetry of $[P_{in} - (P_{in})_o][P_{i'n'} - (P_{i'n'})_o]$ as is described by the multiplication table, Table 5, for parameters symmetrized using the coefficients $\chi_{\rm mn}$ described in Table 4.

However, symmetrized parameters for the doubly degenerate $C\bar{1}$ modes can be chosen in a number of ways and the choice is best made by taking actual notice of the structure.

A2. Choice of variables for constrained refinement

Pseudo-equivalent positions $x,y + \frac{1}{4},z + \frac{1}{2}$; $x,y + \frac{3}{4},z + \frac{1}{2}$; $-x + \frac{1}{4},y + \frac{1}{2},-z$; $-x + \frac{1}{4},y,-z$ may be re-described as x,y,z; $x,y + \frac{1}{2},z$; $-x + \frac{1}{4},y + \frac{1}{4},-z + \frac{1}{2}$; $-x + \frac{1}{4},y + \frac{3}{4},-z + \frac{1}{2}$ acting on $x',y',z' = x,y + \frac{1}{4},z + \frac{1}{2}$ rather than x,y,z. Thus, we can use symmetrized variables suggested by the subgroup $P2_1/n$, where all parameters are associated with the pseudo-equivalent positions x,y,z; $x,y + \frac{1}{2},z$; $-x + \frac{1}{4},y + \frac{1}{4},-z + \frac{1}{2}$; $-x + \frac{1}{4},y + \frac{3}{4},-z + \frac{1}{2}$. Values of χ_{mn} are now those of Table 6.

We now produce the results $I(\mathbf{H}) = |F_1(\mathbf{H})|^2 + |F_2(\mathbf{H})|^2$ for h even, k even reflections and $I(\mathbf{H}) = |F_3(\mathbf{H})|^2 + |F_4(\mathbf{H})|^2$ for h odd, k odd reflections and $|F_1(\mathbf{H})|^2 = 0$ for the systematic absence conditions of the $P2_1/n$ parent structure. The cations are now separated into two subsets. The dominant component for the h even, k even reflections is the $P2_1/n$ component, but the dominant $C\bar{1}$ component is yet to be determined. It should be noted that $I(\mathbf{H}) = |F(\mathbf{H})|^2 + |F(\mathbf{2H})|^2$ and values for χ_{m3} of $2^{1/2}$, $-(2)^{1/2}$, 0, 0 and for χ_{m4} of 0, 0, $(2)^{1/2}$, $-(2)^{1/2}$ makes $F_3(\mathbf{H}) = F(\mathbf{H})$ and $F_4(\mathbf{H}) = (-1)^{h+2k+l}F(\mathbf{2H})$. However, this adds no insight to problems in the structure refinement.

The structure factor is made up of contributions from different asymmetric units of the true structure and the choice as to which of a set of equivalent atoms is in the reference asymmetric unit is irrelevant. However, in a pseudo-symmetric structure the choice of which of a set of pseudo-equivalent atoms is in a pseudo-asymmetric unit becomes important.

Consider the use of the reference position $x',y',z' = -x + \frac{1}{4},y + \frac{3}{4},-z + \frac{1}{2}$ instead of x,y,z. The new pseudo-equivalent positions $1',2',3',4'$ in Table 6 correspond to the old pseudo-equivalent positions 4,3,1,2. What was previously described as a $C\bar{1}^{\rm i}$ component should now be described as a $C\bar{1}^{\rm ii}$ component and what was previously described as a $C\bar{1}^{\rm ii}$ component should now be described as a $C\bar{1}^{\rm i}$ component.

Thus, in the first-order approximation $F_n(\mathbf{H}) \simeq [F_n(\mathbf{H})]_o + \Sigma_i[\partial F(\mathbf{H})/\partial P_{in}]_o[P_{in} - (P_{in})_o]$ we can enforce the dominant $C\bar{1}$ displacive mode for any set of four pseudo-equivalent cations or anions that belong to the $C\bar{1}^{\rm ii}$ component by choosing the appropriate reference cation or anion. Consequently, the first-order approximation of the $C\bar{1}^{\rm i}$ component now contains only the minor displacive mode for each set of ions. (Our choice of a global phase for the $P\bar{1}$ component and our choice of location for a reference cation as the true inversion at $\frac{1}{2}$,0,0 and subsequent comparative refinement implied that our dominant displacement mode should be labelled $C\bar{1}^{\rm ii}$ and not $C\bar{1}^{\rm i}$.)

Subsequent refinement of the origins and the orientations of the cations at the general positions $\sim\frac{1}{2},\frac{1}{4},\frac{1}{2}$ and $\sim\frac{3}{4},\frac{1}{2},0$ showed that a $C\bar{1}^{\rm ii}$ component was dominant for the translation component if the reference molecule was located at $\frac{1}{2},\frac{1}{4},\frac{1}{2}$ and not $\frac{3}{4},\frac{1}{2},0$. The rotational contribution to this component is zero to a first-order approximation, as imposed by the value of -1 for χ_{mn} for inversion at the cation centre. Likewise, for the anions a $C\bar{1}^{\rm ii}$ component was dominant for the translation and rotation components if the reference molecule was located at $\sim$ 5/8,y,0 and not 5/8,$y + \frac{1}{4},\frac{1}{2}$, $y \sim 0.19$ or 0.69.

Since $C\bar{1}^{\rm ii}$ was the dominant component in our choice of structure description, a constraint in the penultimate stage of our hierarchical refinement procedure was to assume no first-order $P\bar{1}$ or $C\bar{1}^{\rm i}$ contribution from changes in local orthonormal coordinates relative to the refinable orthonormal axial systems for the cations. Thus, each pair of pseudo-equivalent positions, *viz.* (x,y,z and $-x + \frac{1}{4},y + \frac{3}{4},-z + \frac{1}{2}$), was constrained to have its own local coordinates in common, where x,y,z refers to a cation at $\frac{1}{2}$,0,0; $\frac{1}{2},\frac{1}{2}$,0; $\frac{3}{4}$,0,0; $\frac{3}{4},\frac{1}{2}$,0. For a reference cation in a general position, the pseudo-inversion related halves of the cation were independent of each other. To a first-order approximation the $P\bar{1}$ and $C\bar{1}^{\rm i}$ components then simply describe small changes in orientation and origin for the cation axial systems that retained a pseudo-equivalence when the $P2_1/n$ and $C\bar{1}^{\rm ii}$ components are considered in isolation. The use of rigid-body models to describe atom displacement parameters also restricts the extent to which differences in atom displacement parameters contribute to the minor components.

Table 7
Multiplication table using a $P2_1/n$ parent structure.

	$P2_1/n$	$P\bar{1}$	$C\bar{1}^{\rm i}$	$C\bar{1}^{\rm ii}$
$P2_1/n$	$P2_1/n$	$P\bar{1}$	$C\bar{1}^{\rm i}$	$C\bar{1}^{\rm ii}$
$P\bar{1}$	$P\bar{1}$	$P2_1/n$	$C\bar{1}^{\rm ii}$	$C\bar{1}^{\rm i}$
$C\bar{1}^{\rm i}$	$C\bar{1}^{\rm i}$	$C\bar{1}^{\rm ii}$	$P2_1/n$	$P\bar{1}$
$C\bar{1}^{\rm ii}$	$C\bar{1}^{\rm ii}$	$C\bar{1}^{\rm i}$	$P\bar{1}$	$P2_1/n$

To understand second-order effects we use the multiplication table, Table 7. As can be seen from Table 7, the $P2_1/n$ and $C\bar{1}^{\rm ii}$ components alone do not induce the $P\bar{1}$ and $C\bar{1}^{\rm i}$ components, nor initiate their refinement. However, the $C\bar{1}^{\rm ii}$ and $P\bar{1}$ components can produce a non-zero contribution to the $C\bar{1}^{\rm i}$ component initiating its refinement. Restricting the nature of the $P\bar{1}$ and $C\bar{1}^{\rm i}$ components allows a sensible refinement pathway before initiating the final refinement stage. Refinement was initiated by a rotation of the cations on true inversion centres using a mode of $P\bar{1}$ symmetry, followed by a mode of $C\bar{1}^{\rm ii}$ symmetry, see earlier.

Omitted second-order terms can be compensated for by the first-order contributions of symmetrized anisotropic atom displacement parameters to the appropriate $F_n(\mathbf{H})$. This was the essence of the hierarchical approach to the refinement used to obtain the structure solution. Atom displacement parameters of a model constrained to retain $P2_1/n$ or $P\bar{1}$ symmetry identified the nature of omitted symmetrized components. The likelihood of mistakes can be assessed by noting the presence or absence of strange anisotropic atom displacement parameters. Mistakes can be compensated by incorrect atom displacement parameters. The use of identical object constraints and rigid-body *TLX* models improved the ability to correct mistakes. It is noted that $[\partial^2 F(\mathbf{H})/\partial P_{in}\partial P_{i'n'}]_o$ is only non-zero if P_{in} and $P_{i'n'}$ involve a common atom. Table 7 shows how the existence of two symmetrized components can induce an $F_n(\mathbf{H})$ component for a third symmetrized component. Each symmetrized component has to have some initial parameterization for $F_n(\mathbf{H}) \neq 0$ in order to make possible the refinement of that component. A poor choice can result in a particular component being predominantly noise and the model for this component is not necessarily improved as refinement proceeds.

We thank Mr Flemming Hansen for help with the crystallographic experiments. Jette Oddershede and Inger Søtofte are thanked for helpful discussions. The work has been supported by the Faculty of Science, University of Copenhagen and the Danish National Science Foundation.

References

Allen, F. H. (2002). *Acta Cryst.* B**58**, 380–388.

Altomare, A., Burla, M. C., Camalli, M., Cascarano, G., Giacovazzo, C., Guagliardi, A., Moliterni, A. G. G., Polodori, G. & Spagna, R. (1999). *J. Appl. Cryst.* **32**, 115–119.
Barra, A.-L., Gatteschi, D. & Sessoli, R. (1997). *Phys. Rev. B*, **56**, 8192–8198.
Blessing, R. H. (1987). *Crystallogr. Rev.* **1**, 3–58.
Bosnich, B., Poon, C. K. & Tobe, M. L. (1965). *Inorg. Chem.* **4**, 1102–1108.
Bradley, C. J. & Cracknell, A. P. (1972). *The Mathematical Theory of Symmetry in Solids: Representation Theory for Point Groups and Space Groups.* London: Oxford University Press.
Daugherty, P. A., Glerup, J., Goodson, P. A., Hodgson, D. J. & Michelsen, K. (1991). *Acta Chem. Scand.* **45**, 244–253.
Duisenberg, A. J. M. (1992). *J. Appl. Cryst.* **25**, 92–96.
Duisenberg, A. J. M., Kroon-Batenburg, L. M. J. & Schreurs, A. M. M. (2003). *J. Appl. Cryst.* **36**, 220–229.
Greenwood, N. N. & Earnshaw, A. (1984). *Chemistry of the Elements*, ch. 19. Oxford: Pergamon Press.
Haller, K. J., Rae, A. D., Heerdegen, A. P., Hockless, D. C. R. & Welberry, T. R. (1995). *Acta Cryst.* B**51**, 187–197.
Johnson, C. K. (1976). *ORTEP*II. Report ORNL-5138. Oak Ridge National Laboratory, Tennessee, USA.
Long, J. (2003). *Chemistry of Nanostructured Materials*, edited by P. Yang, p. 291, Hong Kong: World Scientific Publishing.
Meyer, K., Bendix, J., Metzler-Nolte, N., Weyhermüller, T. & Wieghardt, K. (1998). *J. Am. Chem. Soc.* **120**, 7260–7270.
Mossin, S., Sørensen, H. O. & Weihe, H. (2002). *Acta Cryst.* C**58**, m204–m206.
Mossin, S., Sørensen, H. O.,Weihe, H., Glerup, J. & Søtofte, I. (2005). *Inorg. Chim. Acta*, **358**, 1096–1106.
Nonius (1999). *Collect.* Nonius BV, Delft, The Netherlands.
Rae, A. D. (1975*a*). *Acta Cryst.* A**31**, 560–570.
Rae, A. D. (1975*b*). *Acta Cryst.* A**31**, 570–574.
Rae, A. D. (1984). *Acta Cryst.* A**40**, Suppl. Abstr. 17.4-4, p. 428.
Rae, A. D. (2000). *RAELS*2000. Australian National University, Canberra, Australia.
Rae, A. D. & Willis, A. C. (2003). *Z. Kristallogr.* **218**, 221–230.
Rae, A. D., Withers, R. L., Thompson, J. G. & Willis, A. C. (1990). *Acta Cryst.* B**46**, 474–487.
Sheldrick, G. M. (1997). *SHELXL*97. University of Göttingen, Germany.
Vicente, R., Escuer, A., El Fallah, M. S., Solans, X. & Font-Bardia, M. (1997). *Inorg. Chem. Acta*, **261**, 227–232.